Soft Matter

PAPER

View Article Online
View Journal | View Issue

Cite this: *Soft Matter*, 2026, **22**, 2290

Nonlinear elasticity and transition to macroscopic irreversibility in composite hydrogels

Ippolyti Dellatolas, *[a] Thibaut Divoux, [bc] Emanuela Del Gado [d] and Irmgard Bischofberger *[a]

Received 29th September 2025,
Accepted 17th February 2026

DOI: 10.1039/d5sm00990a

rsc.li/soft-matter-journal

Filler-hydrogel composites combine enhanced mechanical properties with functionalities conferred by the nanofillers. When the nanofillers interact attractively with the hydrogel matrix, even low nanofiller volume fractions can lead to a strong increase in the linear viscoelastic moduli. Here, we build on our understanding of the microscopic phenomena at play in these systems to explore their nonlinear response, using attractive nanofillers embedded in a gelatin matrix. We identify a critical deformation beyond which the material no longer recovers its macroscopic viscoelastic properties, marking the onset of macroscopic irreversibility. Increasing nanofiller volume fraction leads to nanofiller-induced stiffening of the polymer matrix, yet the overall viscoelastic response of the composites remains qualitatively similar to that of pure hydrogels: under increasing strain amplitude, their elastic and viscous moduli, G' and G'', exhibit a pronounced overshoot followed by a crossover associated with yielding. A transition occurs in the composite at the strain amplitude γ'_{max} where G' reaches its maximum, characterized by a marked change in the stress relaxation dynamics. Beyond γ'_{max}, the composites no longer recover their initial viscoelastic properties in repeated strain amplitude sweeps, indicating that the material has sustained macroscopically irreversible changes and a permanent loss of elasticity. We thus identify three distinct regimes in the strain-stiffening materials: nonlinear elasticity, macroscopic irreversibility, and yielding. We further suggest that the plasticity underpinning macroscopic irreversibility is due to the breaking of bonds that contribute most to the composite's strain stiffening response in the hydrogel matrix.

Introduction

The ability of materials to undergo plastic deformation is exploited in applications such as 3D printing, where the viscoelastic response of inks enables high resolution and varied patterns in direct ink writing,[1,2] in bioinks, where the plasticity of hydrogels enhances cell spreading and migration in cell cultures,[3] or in injectable hydrogels for drug and cell delivery.[4,5] Hydrogels, composed primarily of water, are indeed particularly relevant in medical applications due to their potential biocompatibility.[6–9] Incorporating nanofillers at low volume fractions can improve their mechanical properties and introduce specific functionalities.[10–14] Understanding how these materials respond to increasingly large deformations is key to fine-tuning their behavior to a desired application.[15–17] In particular, identifying the onset and mechanisms of permanent damage, at both a microscopic and a macroscopic level, is essential when composites undergo repeated loading.

A material that experiences small deformations or loads can fully recover its original state once the deformation or load is removed.[18] This behavior defines the elastic regime. As the deformation becomes larger, the material undergoes irreversible microscopic rearrangements, marking the transition to the plastic regime.[19] The onset of plasticity corresponds to the strain at which the transition between the elastic regime and the plastic regime occurs and is typically defined for a given system based on a specific rheological test – for example as the deviation from a linear stress response in shear startup or in large-amplitude oscillatory strain sweeps.[20–22] Yielding, which marks the transition from a solid-like state to one where the material flows or fractures, occurs beyond the onset of plasticity.[23] Previous work on the nonlinear behavior of soft materials has explored the microscopic origin of yielding in soft glassy materials, *i.e.*, amorphous soft solids and densely packed systems, as well as in colloidal gels,[24–34] revealing that local plastic events generally precede yielding.[35] In yield stress fluids, which flow only beyond a critical stress,[36] the material can accumulate strain either through recoverable elastic deformation or through unrecoverable plastic deformation.[37,38] While yielding has in general been ascribed to a sharp transition from

[a] *Department of Mechanical Engineering, Massachusetts Institute of Technology, Cambridge, MA 02139, USA. E-mail: ippolyti@mit.edu, irmgard@mit.edu*
[b] *ENSL, CNRS, Laboratoire de Physique, F-69342 Lyon, France*
[c] *International Research Laboratory, French American Center for Theoretical Science, CNRS, KITP, Santa Barbara, USA*
[d] *Department of Physics and Institute for Soft Matter Synthesis and Metrology, Georgetown University, Washington, DC 20057, USA*

a solid-like to a liquid-like state,[22,23,36] it can be more gradual in systems where the viscous modulus G'' exhibits an overshoot as the strain transitions from recoverable to unrecoverable with increasing deformation.[37] Within this framework, yielding is linked to the progressive accumulation of plasticity through local structural rearrangements, associated with the overshoot of the viscous modulus G''. The amount of plastic deformation acquired before yielding determines whether the material exhibits brittle or ductile failure, where brittle failure is often associated with abrupt fracture as opposed to progressive yielding characteristic of ductile failure.[39,40] The impact of progressive plasticity on a material's elasticity and its ability to recover its viscoelastic response under increasing deformation – termed macroscopic reversibility[28] – remain largely unexplored, particularly in materials that exhibit strain stiffening prior to yielding.

Here, we report on the nonlinear elasticity, macroscopic irreversibility, and yielding in composite hydrogels that exhibit an overshoot in both the elastic modulus (associated with strain stiffening) and the viscous modulus with increasing strain amplitude. These overshoots occur in the range of strain amplitudes between the linear elastic regime and the yield point, defined as the crossover of the elastic and viscous moduli. Such a non-monotonic viscoelastic response is commonly observed in hydrogels and other biopolymer soft solids.[41–44] The distinct sequence of viscoelastic regimes occurring with increasing strain amplitude – linear elastic, strain stiffening, and yielding – provides a framework for understanding the interplay between microscopic plasticity, damage accumulation, and macroscopic irreversibility.

We identify a critical strain beyond which the system transitions from a macroscopically reversible to a macroscopically irreversible response. Remarkably, this critical strain coincides with the strain γ'_{max} at which G' reaches its maximum. Below this threshold, the material fully recovers its viscoelastic properties, indicating that the deformation does not significantly alter the microstructure in a way that impacts the macroscopic response. This suggests the existence of a nonlinear and yet fully elastic regime, whose upper bound is set by γ'_{max}. This critical strain is significantly smaller than the yield strain defined as the crossover of G' and G''.[22] We propose that the macroscopic irreversibility observed beyond γ'_{max} arises from the breakage of bonds responsible for the material's nonlinear elasticity. This understanding offers new insights on strain stiffening materials and raises the question of how macroscopic irreversibility occurs more generally, particularly in systems exhibiting a monotonic decrease in G'. Our findings can guide the design of hydrogel composites by identifying the critical strain, specific to the material, beyond which its microstructure and macroscopic viscoelastic properties are permanently affected.

Methods

Sample preparation

The hydrogel composites consist of carboxylate-modified polystyrene nanofillers (CA100NM, Magsphere) of radius $r_f = 50$ nm embedded in gelatin type B (G9391, Sigma Aldrich) hydrogels. The PS nanofillers are carboxyl-coated and negatively charged (0.12 meq g^{-1}). Gelatin type B is amphoteric (pI = 4.7–5.3), leading to weakly negative or near-neutral chains at the working pH (5–7). The interactions between nanoparticles and gelatin are attractive with gelatin due to electrostatic and hydrophobic contributions.[45–48] The gelatin is dissolved in deionized water at concentrations ranging from c_{gel} = 10–18 wt% under continuous stirring at 80 °C for 20 minutes. The nanofillers are added to the hot aqueous solution at volume fractions ϕ_f varying between 5×10^{-4} and 0.09. The hydrogel forms upon cooling in the presence of the nanofillers.

Rheological measurements

Rheological tests are conducted in a parallel-plate geometry (diameter d = 40 mm, initial gap height h_0 = 500 μm) connected to a strain-controlled rheometer (ARES-G2, TA Instruments). The geometry is coated with a trizact self-adhesive abrasive disc (1700 grit, 3 M) to prevent wall slip. We maintain $F_N = 0 \pm 1$ N throughout gelation to compensate for sample contraction or gap decrease induced by gel formation, which would create artificial pre-stresses known to impact the nonlinear response of gels.[21] Hot gelatin samples containing nanofillers are placed in the pre-heated geometry. The samples are sealed with mineral oil (330779, Sigma-Aldrich) to prevent evaporation. The gelation is induced by decreasing the temperature at 5 °C min^{-1} from 80 °C to 25 °C. The sol–gel transition is monitored for 30 minutes at a strain amplitude $\gamma_0 = 0.01$ and frequency $\omega = 2\pi$ rad s^{-1}. We then perform one of the following rheological tests: a strain amplitude sweep, a stress relaxation test, a two-step stress relaxation test, or a series of successive strain amplitude sweeps. In strain amplitude sweeps, the strain amplitude is progressively increased from $\gamma_0 = 0.005$ to $\gamma_0 = 50$ at $\omega = 2\pi$ rad s^{-1}. In stress relaxation experiments, a fixed strain is applied, and the stress response is recorded for 20 minutes. In two-step stress relaxation experiments, an initial strain γ_1 is imposed, and the stress response is recorded for 20 minutes. This is followed by a 10 minute time sweep at $\gamma_0 = 0.01$ and frequency $\omega = 2\pi$ rad s^{-1} to monitor the viscoelastic properties of the composite. A second stress relaxation step is then performed by imposing a strain of amplitude γ_2 of equal magnitude and same direction ($\gamma_2 = \gamma_1$). In the strain amplitude sweep series, we alternate between an amplitude sweep at $\omega = 2\pi$ rad s^{-1} from $\gamma_0 = 0.05$ to a maximum final value γ_f and a 5-minute time sweep in the linear regime at $\gamma_0 = 0.01$ and $\omega = 2\pi$ rad s^{-1}. This sequence is repeated four times.

Results

Strain sweep response of composite hydrogels

Our hydrogels exhibit a complex rheological response for increasing strain amplitude, as shown in Fig. 1A where we report the elastic and viscous moduli of a pure gelatin hydrogel with a gelatin concentration c_{gel} = 10 wt% and of a composite gelatin hydrogel with identical gelatin concentration but with a

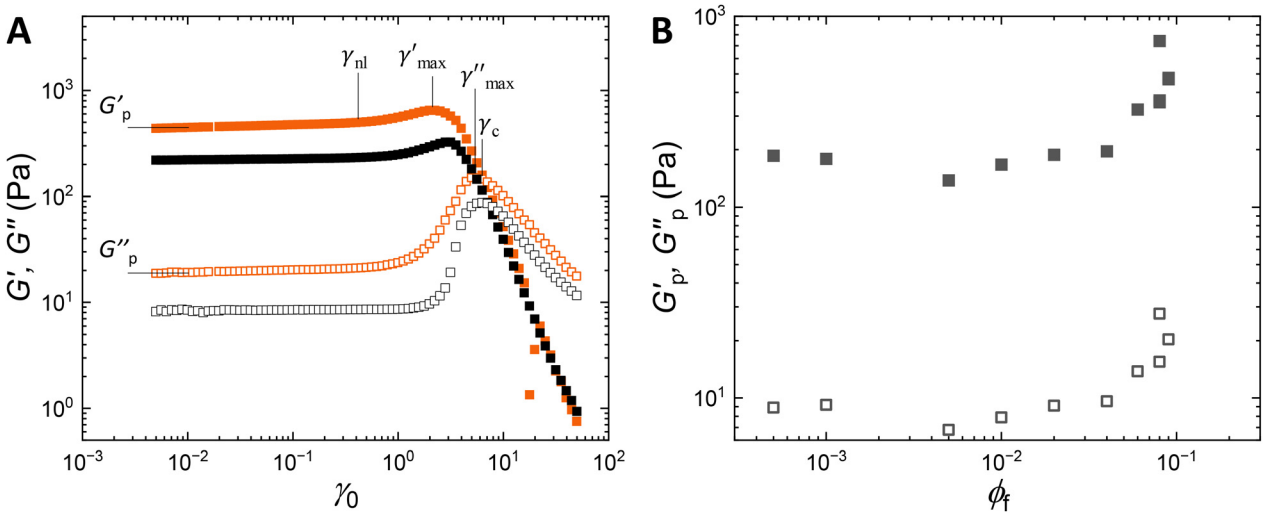

Fig. 1 Strain sweep response of the hydrogels. (A) Elastic modulus G' (closed symbols) and viscous modulus G'' (open symbols) of gelatin hydrogels with gelatin concentration c_{gel} = 10 wt% containing no nanofillers (black symbols) and containing a volume fraction of nanofillers ϕ_f = 0.09 (orange symbols) as a function of strain amplitude γ_0. (B) Reinforcement of the plateau elastic modulus G'_p and the plateau viscous modulus G''_p with increasing volume fraction of nanofillers ϕ_f.

nanofiller volume fraction ϕ_f = 0.09. At low strain amplitudes, both systems display a linear regime, where G' and G'' are independent of the strain amplitude γ_0, up to the strain amplitude denoting the onset of nonlinearity γ_{nl}, defined as the value beyond which G' and G'' are no longer constant. The elastic modulus is more than an order of magnitude larger than the viscous modulus, indicating that the material's response is primarily elastic. As the strain amplitude increases, the hydrogel undergoes strain stiffening, with G' increasing and reaching a maximum at $\gamma_0 = \gamma'_{max}$. Similarly, G'' increases and reaches a maximum at a higher strain amplitude $\gamma_0 = \gamma''_{max} > \gamma'_{max}$. Beyond these maxima, both G' and G'' decrease and eventually cross at the strain amplitude $\gamma_0 = \gamma_c$. Beyond this crossover point, G'' exceeds G', indicating that the material has yielded.

The overall behavior of pure and composite gelatin hydrogels is similar; both materials exhibit a linear regime, followed by strain stiffening and yielding with increasing strain amplitude. Increasing the nanofiller volume fraction, however, significantly enhances the elastic and viscous moduli in the linear regime, G'_p and G''_p, with a fivefold increase for $\phi_f \approx 0.09$, as shown in Fig. 1B. The reinforcement originates from attractive interactions between the nanofillers and the surrounding hydrogel matrix, specifically electrostatic interactions between the gelatin and the polystyrene nanofillers.[45,46] This attraction leads to a local hydrogel densification around the nanofillers, as discussed in our previous work.[10] Microscopic evidence of this densification is provided through small-angle X-ray scattering experiments and atomic force microscopy experiments, as discussed in Fig. S1 of the SI. We showed that these densified regions act as 'effective fillers', which, at sufficiently high nanofiller concentrations, form a percolated network that enhances the stress transmission throughout the material. This network restricts thermal fluctuations of the gel strands, leading to a global stiffening of the composite hydrogel.[10]

Onset of nonlinearities in composite hydrogels

The strain response of composite hydrogels with increasing nanofiller content (ϕ_f = 0.0005–0.09) and of pure gelatin hydrogels with increasing gelatin concentration (c_{gel} = 10–18 wt%) are shown in Fig. 2A and B. The elastic modulus increases with increasing nanofiller volume fraction and gelatin concentration. Adding nanofillers shifts the onset of nonlinearity to lower strain amplitudes compared to pure hydrogels. In particular, γ'_{max} decreases with increasing nanofiller volume fraction, whereas it remains nearly unchanged with increasing gelatin concentration, as shown in Fig. 2C where we report γ'_{max} as a function of the plateau modulus G'_p to show that the decrease in γ'_{max} is not simply due to an increase in the gel linear elastic modulus that increases as a power law with gelatin concentration.[49] Other critical strains, including γ_{nl}, γ_c, and γ''_{max}, exhibit a similar decreasing trend with increasing nanofiller volume fraction, as shown in Fig. S2 in the SI. In contrast, the relative amplitude of strain stiffening, defined as the normalized increase in G' relative to the modulus at the onset of nonlinearity, $\Delta G'/G'_{nl} = (G'_{max} - G'_{nl})/G'_{nl}$, depends only on the gel elastic modulus (SI Fig. S3): for a given gel modulus, the amplitude of strain stiffening is the same in both composite and pure gelatin hydrogels.

The observation that strain stiffening occurs at the same strain in pure gelatin gels across a concentration range of c_{gel} = 10–18 wt% reveals that it is not governed by the crosslink density or the mesh size of the hydrogel. Instead, the strain stiffening likely originates from a local nonlinear response of the gelatin chains due to a transition from bending to stretching of the chains under increasing strain.[50,51] Indeed, strain stiffening has been observed in various hydrogels and biological systems, where it is commonly attributed to the nonlinear response of individual polymer chains under high extension.[52–55] The onset of strain stiffening correlates with the persistence length of the

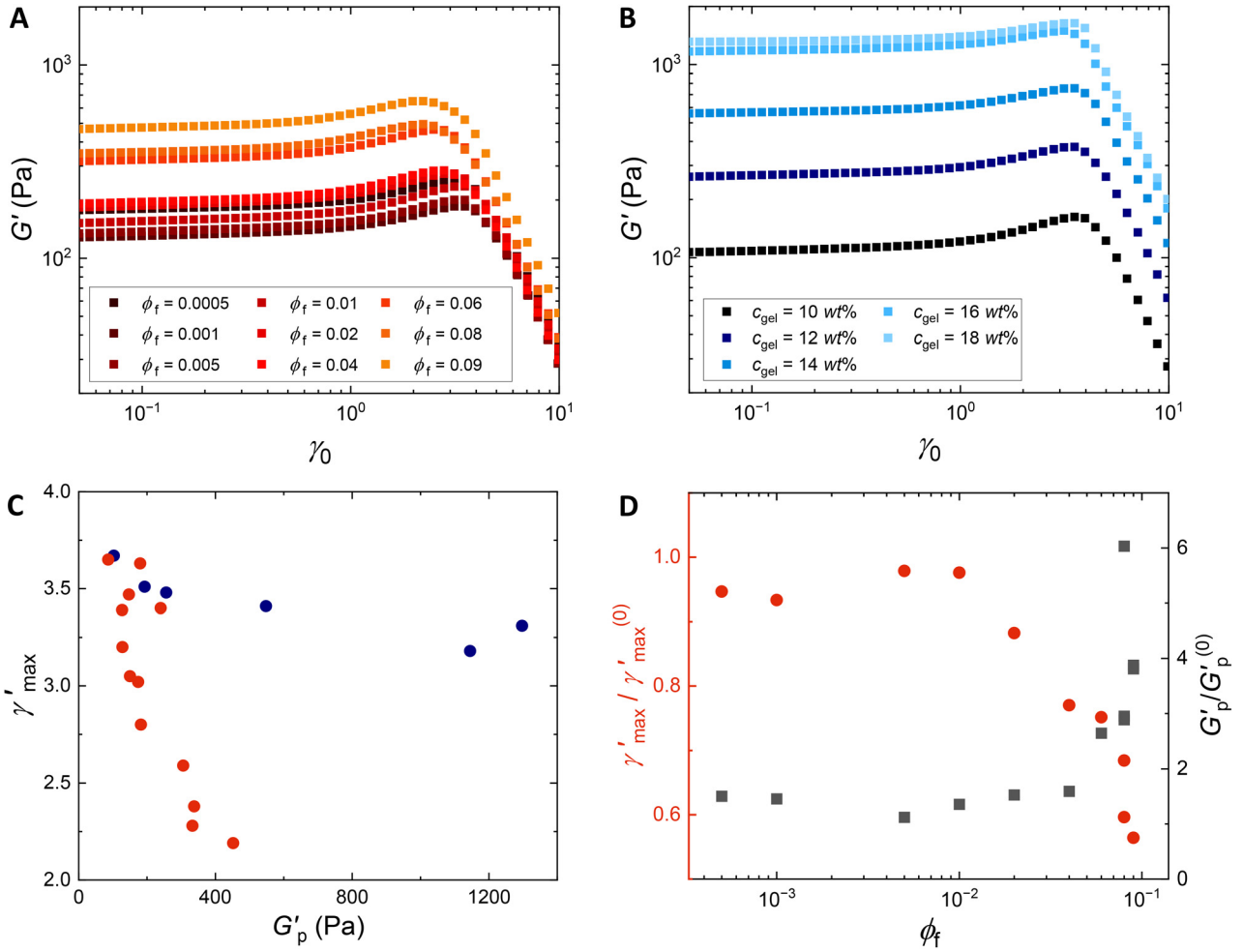

Fig. 2 Strain sweep response of composites and pure gels. Elastic modulus G' of (A) filler-gelatin composites with gelatin concentration c_{gel} = 10 wt% and nanofiller volume fractions ranging from ϕ_f = 0.0005 to 0.09 and (B) pure gelatin hydrogels with concentrations ranging from c_{gel} = 10 wt% to 18 wt%. (C) The strain γ'_{max} at which G' reaches a maximum decreases with increasing gel plateau modulus G'_p in composite hydrogels (red symbols), but remains almost constant in pure gelatin hydrogels (blue symbols). (D) Left axis: strain γ'_{max} of the composite hydrogel, normalized by $\gamma'_{max}{}^{(0)}$ of the pure gelatin hydrogel. Right axis: elastic modulus of the composite hydrogel normalized by that of the pure gelatin hydrogel, $G'_p/G'^{(0)}_p$, as a function of nanofiller volume fraction ϕ_f.

polymer chains, with stiffer chains exhibiting stiffening at lower strains compared to more flexible ones.[42] In our composite hydrogels, the shift in the onset of strain stiffening suggests that the addition of nanofillers reduces chain extensions, making lower strains sufficient to trigger a nonlinear response. Notably, the nanofiller volume fraction beyond which the critical strains decrease is close to the volume fraction denoting the onset of reinforcement, as shown in Fig. 2D. Our previous work revealed that the hydrogel locally densifies around the nanofillers. This densified shell acts as a mechanically stiffer region. As the number of these regions grows, they begin to overlap and form a percolated structure that constrains the thermal fluctuations of the surrounding gel strands.[10] This suppression of fluctuations stiffens the effective network segments, resulting in an overall increase in the composite modulus. This is consistent with a reduction of chain extensions at these volume fractions and a decrease in the critical strains. Once this strain denoting the onset of strain stiffening is reached, the magnitude of strain stiffening depends only on the gel modulus, as the nature of the gelatin chains remains unchanged.

The observation that the overall behavior of the elastic and viscous moduli across the linear, strain-stiffening, and yielding regimes remains similar across gels with different nanofiller content and in the pure gelatin hydrogels suggests that the microscopic phenomena governing the viscoelastic response primarily occur within the polymer matrix, rather than being caused by the nanofillers.

Transition beyond nonlinear elasticity

To further probe the nonlinear response of the hydrogels, we perform stress relaxation experiments where we record the stress response $\sigma(t)$ to a step strain of amplitude γ_0. We select strain values in three regimes: the linear regime, the strain-stiffening regime, and beyond the maximum of G'. To account for the shift in critical strain amplitudes induced by the

nanofillers, we define the reduced strain amplitude $\gamma_0^* = \gamma_0 - \gamma'_{max}$ to report the relaxation modulus $G(t) = \sigma(t)/\gamma_0$ for varying imposed strain amplitudes γ_0, as shown in Fig. 3A.

For $\gamma_0^* < 0$ (before the peak in G'), $G(t)$ exhibits a single decay, with nearly identical responses in both the linear and strain-stiffening regimes. Conversely, for $\gamma_0^* > 0$ (beyond the peak in G'), the relaxation modulus exhibits a multi-step decay: an initial rapid drop followed by a long-time relaxation similar to that observed at lower strains. At long times, when rescaled by a factor $A(\gamma_0)$, the relaxation modulus for all strain amplitudes collapses onto a master curve that exhibits a stretched exponential decay (gray curve in Fig. 3B). At short times, the stress response exhibits a very rapid decay that is faster than the response time of the rheometer. This is evidenced by the fact that the first reported value of the relaxation modulus is lower than the plateau modulus of the hydrogel prior to the stress relaxation. Within the measurable time window, the relaxation exhibits a power-law decay with an exponent k that becomes increasingly negative with increasing strain amplitude, as shown in Fig. 3C. The scaling factor A captures the effect of both these early-time decays, as it sets the height of the plateau of the stretched exponential decay relative to the plateau elastic modulus of the hydrogel G_p. The ratio A/G_p decreases with increasing γ_0^* (Fig. 3D), indicating that the

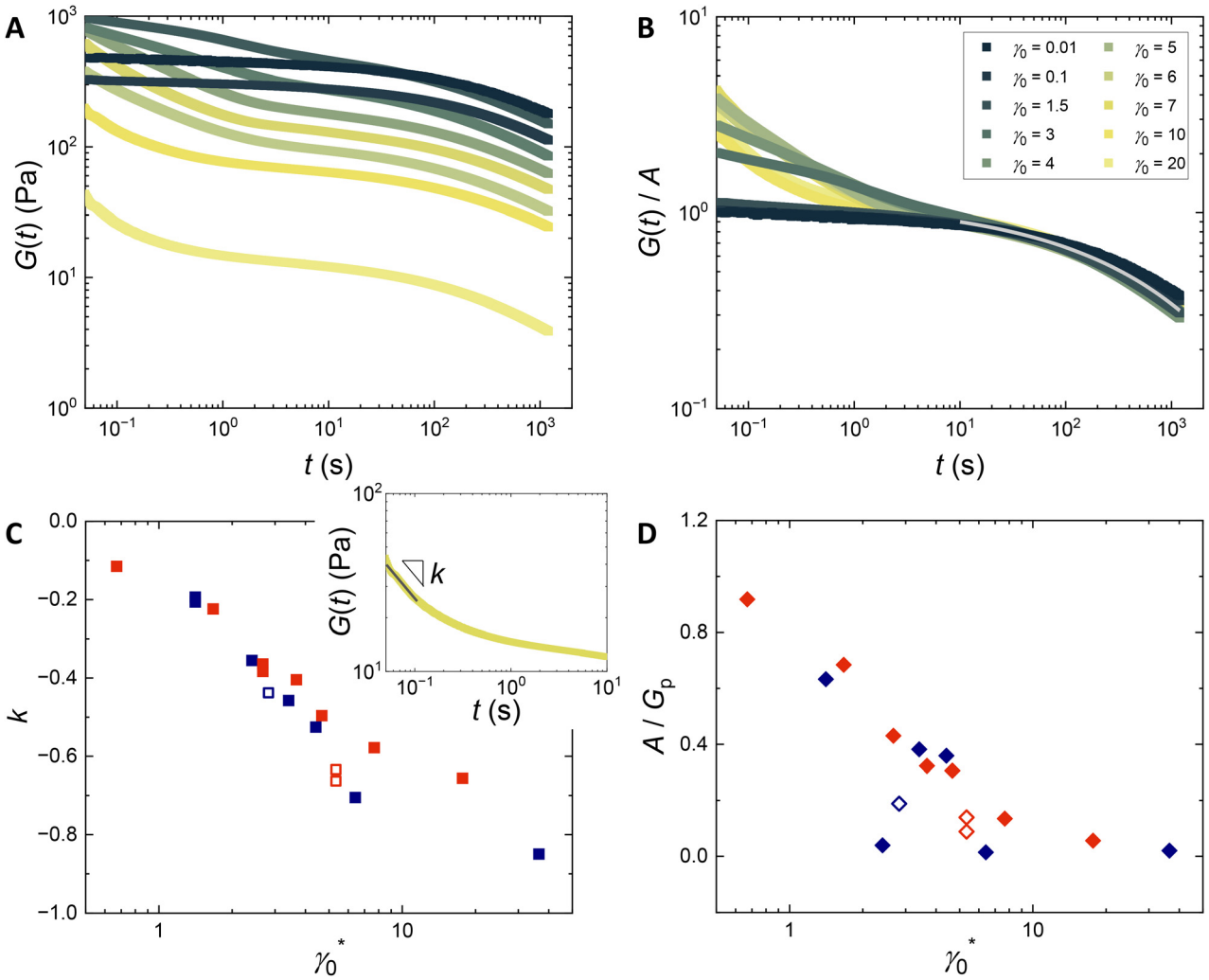

Fig. 3 Stress relaxation. (A) Relaxation modulus $G(t) = \sigma(t)/\gamma_0$ of a composite hydrogel (c_{gel} = 10 wt%, ϕ_f = 0.08) for which $\gamma'_{max} = 2.33$, for different imposed strain amplitudes γ_0. (B) Normalized relaxation modulus $G(t)/A$, with a normalization value $A(\gamma_0)$ chosen such that the late-time response exhibits a master curve for all applied strain amplitudes. The gray curve denotes a stretched exponential fit, $G(t)/A = G_0\exp[-(t/t_0)^\alpha]$, with G_0 = 1.15 Pa, t_0 = 567 s, and α = 0.35 that highlights the universal late-time decay for $t \gtrsim 10$ s. (C) Power-law exponent k of the early-time decay of $G(t)$ as a function of representative strain amplitude $\gamma_0^* = \gamma_0 - \gamma'_{max}$ for the composite hydrogel (red symbols) and the pure hydrogel (blue symbols). The open symbols denote the power-law exponent of the early-time decay of $G(t)$ during the second relaxation step in two successive stress relaxation experiments (as shown in Fig. 4), where each step is performed at a strain γ_1^*, plotted such that for these experiments $\gamma_0^* = 2 \times \gamma_1^*$. Inset: Power-law fit of the early-time decay of $G(t)$ for $\gamma_0^* = 17.67$. (D) Scaling factor $A(\gamma_0)$ normalized by the plateau modulus of the gels G_p *versus* γ_0^* for the composite hydrogel (red symbols) and the pure hydrogel (blue symbols). The open symbols correspond to the normalized scaling factor A/G_p during the second relaxation step in two successive stress relaxation experiments, plotted similarly as in (C).

combined effect of the first decay (inaccessible due to instrument limitation) and the subsequent power-law decay results in a larger initial stress relaxation for higher strain amplitudes.

In pure gelatin gels, the stretched exponential decay has been attributed to a slow coil-to-helix transition of the gelatin strands under shear,[56,57] which we would also expect in the composite hydrogels. We associate the short-time stress relaxation with the breaking of elastically active bonds, where the most "pre-stretched" bonds break first upon the application of strain. The transition from a single-step to a multi-step relaxation occurring at γ'_{max} suggests a transition to a different nonlinear regime. γ'_{max} delineates a nonlinear elastic regime – which extends up to the maximum of strain stiffening – from one that is no longer purely elastic and that emerges beyond the maximum. A similar transition, from a single stretched exponential decay to a multi-step relaxation, has been reported in telechelic associating polymers, where heterogeneity in end-to-end chain distances leads to a distribution of bond breakage probabilities.[53] This supports our suggestion that the short-time stress relaxation stems from the breaking of the most "pre-stretched" bonds, as gelatin is known to form a loosely connected, heterogeneous network of triple helices, with a range of end-to-end distances.[49,58,59] Comparing the stress relaxation profile of composites and pure gelatin gels, we find that both the power-law exponent of the early decay and the rescaling factor A depend similarly on the reduced strain amplitude γ_0^*, as shown in Fig. 3C and D. This suggests that, once the shift in critical strains induced by the nanofillers is accounted for, the nonlinear response at a given strain amplitude is primarily dictated by the gelatin matrix: the bonds responsible for the early-time relaxation correspond to gelatin bonds, rather than interactions introduced by the nanofillers.

To further investigate the transition occurring at γ'_{max}, we perform a two-step stress relaxation experiment. A fixed strain amplitude is applied for 20 minutes, followed by a 10 minute time sweep at a strain amplitude in the linear regime, after which a second stress relaxation experiment is conducted at the same strain amplitude, in the same direction as the first step ($\gamma_2 = \gamma_1$). When the applied strain amplitude lies within the nonlinear elastic regime $(\gamma_1^* < 0)$, the stress relaxation response remains unchanged: both relaxation curves exhibit a single, long-time decay, with no significant differences between the two steps, as shown in Fig. 4A. This suggests that the material retains its ability to recover from deformation within this regime. In contrast, when the strain amplitude exceeds the nonlinear elastic regime $(\gamma_1^* > 0)$, the second relaxation step exhibits a steeper initial decay compared to the first step, while the long-time behavior remains unchanged, as shown in Fig. 4B. The exponent of the initial decay in the second step is reported in Fig. 3C for comparison with the power-law exponents in single-step relaxation experiments. This exponent is of the order of what would be obtained by performing a step strain at an amplitude equal to the sum of the imposed amplitude in each step of the two-step relaxation experiments. This steeper decay in the second step indicates that the first stress relaxation induces permanent structural changes in the material, including irreversible bond breakage and residual bond stretching. As a result, additional bond breakage occurs during the second relaxation, leading to a more pronounced initial relaxation response.

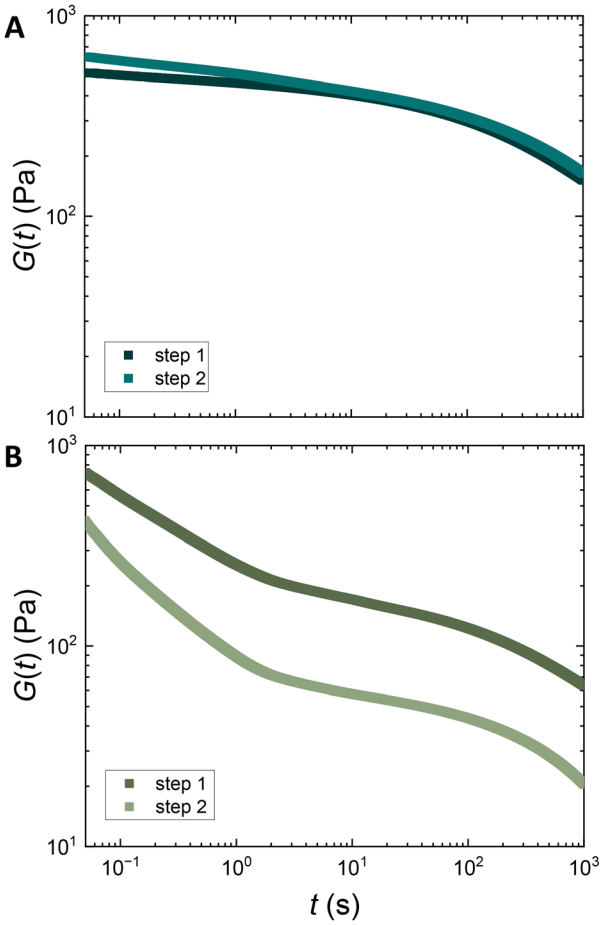

Fig. 4 Two successive stress relaxation experiments. Relaxation modulus $G(t) = \sigma(t)/\gamma_0$ of a composite hydrogel (c_{gel} = 10 wt%, ϕ_f = 0.08) in two successive stress relaxation tests for a strain (A) $\gamma_2^* = \gamma_1^* = -0.83$ in the nonlinear elastic regime and (B) $\gamma_2^* = \gamma_1^* = 2.67$ in the macroscopically irreversible regime.

Manifestation of macroscopic irreversibility

The transition beyond nonlinear elasticity and its relation to irreversible phenomena is further probed by performing a series of repeated strain amplitude sweeps. The strain amplitude is increased from γ_0 = 0.005 to a final value γ_f, followed by a five-minute time sweep in the linear regime. This protocol is repeated for a total of four times, with γ_f chosen either within the strain stiffening regime or beyond γ'_{max}. To account for the aging of the hydrogel during the strain amplitude series, we report an additional control experiment: a time sweep of equivalent duration to the first three strain amplitude series, followed by a strain amplitude sweep performed at the same time as the fourth and final strain sweep in the series. This allows us to isolate the effects of strain history from those of

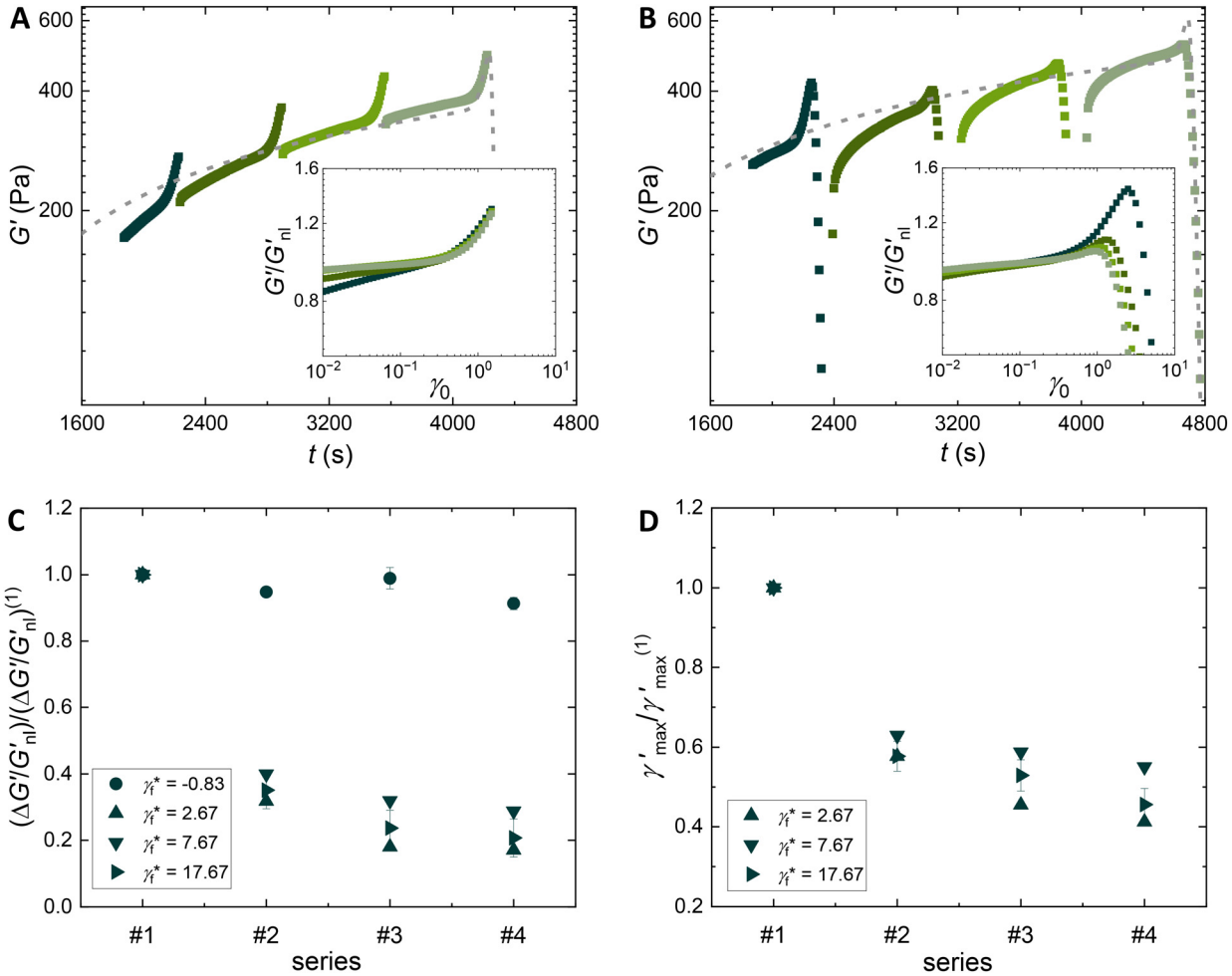

Fig. 5 Strain stiffening in strain amplitude sweep series. Elastic modulus G' as a function of time t during a series of strain sweeps on a composite gelatin hydrogel with a nanofiller volume fraction of ϕ_f = 0.08 and a gelatin concentration of c_{gel} = 10 wt%. The strain amplitude is varied in each strain sweep between (A) γ_0 = 0.005 and γ_f = 1.5 or (B) γ_0 = 0.005 and γ_f = 20. γ'_{max} for this composite is 2.33. The gray dashed line represents the elastic modulus in a separate experiment during a time sweep followed by a strain amplitude sweep, for comparison with the strain amplitude sweep of a gel that has aged for a similar amount of time as the time it takes to perform the first three series. Insets: Elastic modulus normalized by the modulus at the onset of nonlinearity G'/G'_{nl} for each strain sweep as a function of strain amplitude γ_0. (C) The extent of strain stiffening characterized by $\Delta G'/G'_{nl} = (G'_{max} - G'_{nl})/G'_{nl}$ and (D) the strain γ'_{max} at the maximum of G' for each strain amplitude series, normalized by the value from the first series denoted by the superscript (1), for different reduced strain amplitudes γ_f^*.

aging by comparing the final sweep in the series with that of an aged, unstressed gel.

When $\gamma_f < \gamma'_{max}$, the elastic modulus G' exhibits the same behavior across all strain sweeps in the series: the linear regime is followed by strain stiffening, with both the onset and extent of stiffening remaining unchanged, as shown in Fig. 5A. When $\gamma_f > \gamma'_{max}$, however, notable changes occur in subsequent sweeps, as seen in Fig. 5B. Although the gel ultimately recovers its linear elasticity, the magnitude of strain stiffening characterized by $\Delta G'/G'_{nl} = (G'_{max} - G'_{nl})/G'_{nl}$ decreases with each strain sweep, and γ'_{max} shifts to lower values (Fig. 5C and D). In the final strain amplitude sweep, the magnitude of strain stiffening is significantly lower than that of the aged gel. Furthermore, the time needed for the hydrogel to recover its linear viscoelastic properties increases with the maximum strain amplitude in the strain sweeps γ_f, as shown in Fig. S4 in the SI. These observations are consistent with a scenario in which the bonds that break preferentially are those that contribute most significantly to the nonlinear elastic response. Indeed, the decrease in strain stiffening across repeated sweeps indicates that fewer bonds capable of contributing to this response remain intact. At the same time, the recovery of the linear regime in each sweep indicates that the overall material structure remains largely preserved. Since strain stiffening is attributed to the initially stiffer – or more "pre-stretched"– bonds, the results imply that when the gel is strained beyond γ'_{max}, it undergoes plastic deformation, characterized by the irreversible breaking of these most pre-stretched bonds in the gelatin matrix.

The viscoelastic response of the viscous modulus G'' during repeated strain amplitude sweeps is shown in Fig. 6 for varying γ_f. When $\gamma_f < \gamma_c$ (*i.e.*, below the strain characterizing the crossover of G' and G''), the magnitude of the overshoot in G'' remains unchanged across successive strain sweeps. When

$\gamma_f > \gamma_c$, however, the magnitude of the overshoot progressively decreases with each sweep, as shown in Fig. 6B and C. This suggests that while straining the gel into the macroscopically irreversible regime $\gamma_f > \gamma'_{max}$ does not change subsequent viscoelastic energy dissipation, the additional viscoelastic dissipation associated with the overshoot at yielding is reduced once the gel has been strained beyond the yield point. In contrast, the strain amplitude at which the overshoot occurs decreases at each step in the series for strains $\gamma_f > \gamma'_{max}$, as shown in Fig. 6D. This shows that once the gel has been brought into the macroscopically irreversible regime, the strain-induced dissipation associated with yielding decreases. The overshoot in G'' has previously been identified as a signature of unrecoverable strain accumulation through viscoplastic energy dissipation, associated with the buildup of plasticity.[37] The steepness of the overshoot has been linked to microstructural heterogeneities within the gel, with a steeper overshoot indicative of a greater number of locally stiff regions relative to the bulk.[39] These stiff regions hinder the propagation of deformation fields, leading to more abrupt failure. In our experiments, the steepness of the G'' overshoot is similar for each series, suggesting that viscoplastic dissipation and plastic strain accumulation are not significantly affected by the gel's mechanical history. Our results also indicate that the degree of heterogeneity within the hydrogels is not significantly altered by the successive strain sweeps, suggesting that the bond breakage responsible for macroscopic irreversibility occurs predominantly in the denser regions of the gel network.

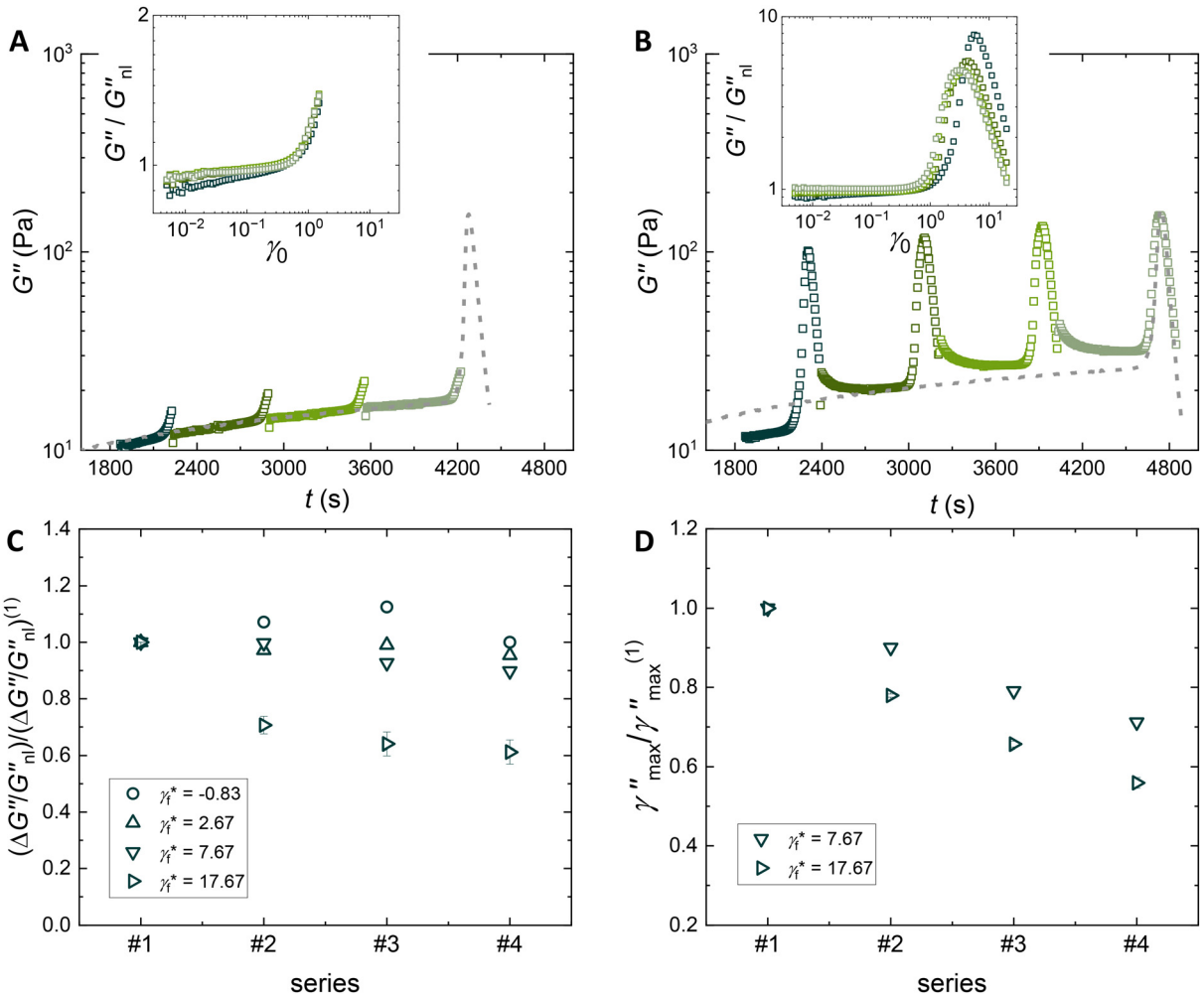

Fig. 6 Viscoelastic dissipation in strain amplitude sweep series. Viscous modulus G'' as a function of time t during series of strain sweeps on a composite gelatin hydrogel with a nanofiller volume fraction of ϕ_f = 0.08 and a gelatin concentration of c_{gel} = 10 wt%. The strain amplitude is varied within each strain sweep between (A) γ_0 = 0.005 and γ_f = 1.5 or (B) γ_0 = 0.005 and γ_f = 20. For this composite, $\gamma'_{max} = 2.33$ and γ_c = 6.11. The gray dashed line represents the viscous modulus in a separate experiment during a time sweep followed by a strain amplitude sweep, for comparison with the strain amplitude sweep of a gel that has aged for a similar amount of time as the time it takes to perform the first three series. Insets: Viscous modulus normalized by the modulus at the onset of nonlinearity G''/G''_{nl} for each strain sweep as a function of strain amplitude γ_0. (C) The extent of the overshoot in G'' characterized by $\Delta G''/G''_{nl} = (G''_{max} - G''_{nl})/G''_{nl}$ and (D) the strain γ''_{max} at the peak of G'' for each strain sweep, normalized by the value from the first series, for different reduced strain amplitudes γ_f^*.

Discussion and conclusions

Plasticity is associated with permanent damage in materials at the microscopic level: the specific microscopic events leading to plasticity accumulation have been studied in a range of materials. However, the impact of plasticity accumulation on macroscopic system mechanics is the subject of ongoing discussion.[38,39] In our hydrogel composites that exhibit strain stiffening, we show that macroscopic irreversibility occurs beyond the strain γ'_{max} corresponding to the maximum of strain stiffening. While the material fully recovers its viscoelastic spectrum after strain amplitude sweeps below γ'_{max}, it does not recover this spectrum after being strained beyond that point. This observation poses a key question: how is macroscopic irreversibility related to microscopically irreversible – or local plastic – events? It is possible that local plastic events occur even below γ'_{max} but remain undetectable at the macroscopic scale. Indeed, a decoupling between microscopic plasticity and macroscopic irreversibility has been observed in a 2D jammed material under shear, where plastic rearrangements precede macroscopic irreversibility – evidenced by changes in the bulk rheology upon reversing the imposed deformation – and rheological yielding.[28] Theoretical work, based on the soft glassy rheology (SGR) model describing elastoplastic yield stress fluids and amorphous soft solids, reported that plastic events contribute to strain recovery when an applied stress is switched off.[32] In our case, the stress relaxation response following a step strain below γ'_{max} is consistent with nonlinear elasticity, while relaxation profiles for strains beyond γ'_{max} are indicative of bond breakage. Notably, this strain is slightly larger than the strain at which the overshoot in G'' begins in our system – a feature commonly used to mark the onset of plasticity in yield stress fluids.[37] This suggests that if damage accumulation occurs within the strain stiffening regime (*i.e.,* below γ'_{max}) through microscopically irreversible local bond failures, these events are either insufficient in number or not spatially organized such that they would manifest macroscopically in stress relaxation experiments or repeated strain amplitude sweeps.

Much work has focused on characterizing failure in materials that exhibit ductile yielding, in contrast to brittle fracture.[39] Yield stress fluids, such as carbopol microgels, tend to fail in a continuous, ductile manner, whereas crosslinked hydrogels or polymer-bridged microemulsions typically exhibit a more abrupt, fracture-like failure. Studies of yielding under creep and steady shear flow emphasize that the type of bonds underlying the gel elasticity and the bond kinetics are critical parameters to predict yielding behavior.[60–62] The physical hydrogels studied in our work could be expected to exhibit a behavior that is neither purely brittle nor purely ductile, as would be the case in a softer, more fluid-like material. Our findings confirm this hypothesis, identifying that beyond γ'_{max}, two types of failure occur simultaneously within the material: a more brittle-like, irreversible, breakage of bonds responsible for the gel's nonlinear elasticity, and a more ductile material response that allows for recovery of the gel's linear viscoelasticity.

A novelty of our work lies in the fact that the materials studied here exhibit an overshoot of G'. This strain-stiffening behavior, common to a range of materials,[42,44] allows us to identify a nonlinear elastic regime between the onset of nonlinearity at γ_{nl} and the peak in G' at γ'_{max}. It would be interesting to consider if and when the transition to macroscopic irreversibility occurs in materials that do not exhibit an overshoot of G'. We would expect macroscopic irreversibility to occur for a strain amplitude between that of the onset of plasticity and that of the crossover of G' and G''. Moreover, strain stiffening in gelatin has been associated with the nonlinear response of the chains that are the most stretched, rather than with plastic effects, such as the formation of new bonds, as the material is deformed, which is consistent with our finding that the strain stiffening regime is nonlinear elastic.[58] A distinction is sometimes made between strain stiffening – where the origin of the increase in G' is nonlinear elastic – and strain hardening – where the origin is plastic – particularly in numerical simulations that can specifically map the network topology.[63,64] It would be interesting to probe the onset of macroscopic irreversibility in strain hardening materials, investigating specifically whether the transition occurs beyond the maximum of G' as in our system, or earlier in the hardening regime.

The hydrogel composites studied here thus exhibit unique features: tunable linear elastic stiffness, the ability to self-heal, and a marked transition from a nonlinear elastic regime where deformations are reversible to a macroscopically irreversible regime where the deformation has permanently affected the material microstructure. This understanding can guide the design of hydrogel composites by identifying the critical strain, specific to the material, beyond which the microstructure and macroscopic viscoelasticity will be permanently affected. The deformation threshold identified in our study beyond which macroscopic irreversibility occurs is related to the strain-stiffening nature of the hydrogel composites. Our results could thus extend to a range of materials that exhibit strain stiffening.

Author contributions

I. D. and I. B. designed the research; I. D. performed the experiments; I. D., T. D., E. D. G., and I. B. interpreted the data; I. D., T. D., E. D. G., and I. B. wrote the paper.

Conflicts of interest

There are no conflicts to declare.

Data availability

All data for this article has been included in the main manuscript and the supplementary information (SI). The SI shows (i) microscopic evidence of local hydrogel densification around the nanofillers based on small-angle-X-ray scattering (SAXS) data and atomic force microscopy (AFM) tests, (ii) the characteristic strains in the viscoelastic response of the composite

hydrogels as a function of the filler volume fraction, (iii) the relative amplitude of strain stiffening in pure hydrogels and composites as a function of the sample elasticity, and (iv) the time to recover linear viscoelasticity in composites hydrogels during strain sweep series. See DOI: https://doi.org/10.1039/d5sm00990a.

Acknowledgements

The authors thank Gavin Donley for helpful discussions. I. D. acknowledges support from a MathWorks Fellowship. T. D. acknowledges support from the Région Auvergne-Rhône-Alpes (AURA) through the Ambition Internationale program and grant NSF PHY-2309135 to the Kavli Institute for Theoretical Physics (KITP). E. D. G acknowledges support from the U.S. National Science Foundation (grant DMREF CBET-2118962) and NSF STC COMPASS (Center for Complex Particle Systems), Award No. 2243104.

References

1 H. Yuk and X. Zhao, *Adv. Mater.*, 2018, **30**, 1704028.
2 Q. Lu, Y. Sun, M. Wu, Q. Wang, S. Feng, T. Fang, G. Hu, W. Huang, Z. Li, D. Kong, X. Wang and Y.-Q. Lu, *ACS Nano*, 2024, **18**, 13049–13060.
3 A. Malandrino, H. Zhang, N. Schwarm, D. Böhringer, D. Kah, C. KusteC, A. Boccaccini and B. Fabry, *Biomacromolecules*, 2024, **25**, 7608–7618.
4 R. Huang, J. Hua, M. Ru, M. Yu, L. Wang, Y. Huang, S. Yan, Q. Zhang and W. Xu, *ACS Nano*, 2024, **18**, 15312–15325.
5 H. Lopez Hernandez, A. K. Grosskopf, L. M. Stapleton, G. Agmon and E. A. Appel, *Macromol. Biosci.*, 2019, **19**, 1800275.
6 Y. Liang, J. He and B. Guo, *ACS Nano*, 2021, **15**, 12687–12722.
7 T. Zhou, H. Yuk, F. Hu, J. Wu, F. Tian, H. Roh, Z. Shen, G. Gu, J. Xu, B. Lu and X. Zhao, *Nat. Mater.*, 2023, **22**, 895–902.
8 C. Xu, Y. Chen, S. Zhao, D. Li, X. Tang, H. Zhang, J. Huang, Z. Guo and W. Liu, *Chem. Rev.*, 2024, **124**, 10435–10508.
9 D. Miranda-Nieves and E. L. Chaikof, *ACS Biomater. Sci. Eng.*, 2017, **3**, 694–711.
10 I. Dellatolas, M. Bantawa, B. Damereau, M. Guo, T. Divoux, E. Del Gado and I. Bischofberger, *ACS Nano*, 2023, **17**, 20939–20948.
11 Z. Meng, Q. Liu, Y. Zhang, J. Sun, C. Yang, H. Li, M. Loznik, R. Göstl, D. Chen and F. Wang, *et al.*, *Adv. Mater.*, 2022, **34**, 2106208.
12 K. Elkhoury, C. S. Russell, L. Sanchez-Gonzalez, A. Mostafavi, T. J. Williams, C. Kahn, N. A. Peppas, E. Arab-Tehrany and A. Tamayol, *Adv. Healthcare Mater.*, 2019, **8**, 1900506.
13 P. Thoniyot, M. J. Tan, A. A. Karim, D. J. Young and X. J. Loh, *Adv. Sci.*, 2015, **2**, 1400010.
14 K. Haraguchi and T. Takehisa, *Adv. Mater.*, 2002, **14**, 1120–1124.
15 A. Z. Nelson, K. S. Schweizer, B. M. Rauzan, R. G. Nuzzo, J. Vermant and R. H. Ewoldt, *Curr. Opin. Solid State Mater. Sci.*, 2019, **23**, 100758.
16 S. Tagliaferri, A. Panagiotopoulos and C. Mattevi, *Mater. Adv.*, 2021, **2**, 540–563.
17 A. Z. Nelson and R. H. Ewoldt, *Soft Matter*, 2017, **13**, 7578–7594.
18 R. Larson, *The Structure and Rheology of Complex Fluids*, Oxford University Press, 1999.
19 N. J. Balmforth, I. A. Frigaard and G. Ovarlez, *Annu. Rev. Fluid Mech.*, 2014, **46**, 121–146.
20 R. Benzi, T. Divoux, C. Barentin, S. Manneville, M. Sbragaglia and F. Toschi, *Phys. Rev. E*, 2021, **104**, 034612.
21 A. Pommella, L. Cipelletti and L. Ramos, *Phys. Rev. Lett.*, 2020, **125**, 268006.
22 R. Cerbino and V. Trappe, *Phys. A: Stat. Mech. Appl.*, 2023, **631**, 128653.
23 H. A. Barnes, *J. Nonnewton. Fluid Mech.*, 1999, **81**, 133–178.
24 G. Negro, L. N. Carenza, G. Gonnella, F. Mackay, A. Morozov and D. Marenduzzo, *Sci. Adv.*, 2023, **9**, eadf8106.
25 D. Pan, T. Ji, M. Baggioli, L. Li and Y. Jin, *Sci. Adv.*, 2022, **8**, eabm8028.
26 P. Leishangthem, A. D. Parmar and S. Sastry, *Nat. Commun.*, 2017, **8**, 14653.
27 J. Lin, E. Lerner, A. Rosso and M. Wyart, *Proc. Natl. Acad. Sci. U. S. A.*, 2014, **111**, 14382–14387.
28 N. C. Keim and P. E. Arratia, *Phys. Rev. Lett.*, 2014, **112**, 028302.
29 N. Koumakis, M. Laurati, S. U. Egelhaaf, J. F. Brady and G. Petekidis, *Phys. Rev. Lett.*, 2012, **108**, 098303.
30 Y. Jin, P. Urbani, F. Zamponi and H. Yoshino, *Sci. Adv.*, 2018, **4**, eaat6387.
31 J. H. Cho and I. Bischofberger, *Soft Matter*, 2022, **18**, 7612–7620.
32 H. A. Lockwood and S. M. Fielding, *J. Rheol.*, 2025, **69**, 329–341.
33 A. Yamamoto, T. Inui, D. Suzuki and K. Urayama, *Soft Matter*, 2023, **19**, 9082–9091.
34 E. L. Jones, Z. Luo, R. Agrawal, S. Flynn, M. Carr, W. N. Sharratt and E. Garcia-Tunon, *Soft Matter*, 2025, **21**, 4822–4838.
35 S. Aime, L. Ramos and L. Cipelletti, *Proc. Natl. Acad. Sci. U. S. A.*, 2018, **115**, 3587–3592.
36 D. Bonn, M. M. Denn, L. Berthier, T. Divoux and S. Manneville, *Rev. Mod. Phys.*, 2017, **89**, 035005.
37 G. J. Donley, P. K. Singh, A. Shetty and S. A. Rogers, *Proc. Natl. Acad. Sci. U. S. A.*, 2020, **117**, 21945–21952.
38 G. J. Donley, S. Narayanan, M. Wade, J. Park, R. Leheny, J. Harden and S. Rogers, *Proc. Natl. Acad. Sci. U. S. A.*, 2023, **120**, e2215517120.
39 M. K. Kamani and S. Rogers, *Proc. Natl. Acad. Sci. U. S. A.*, 2024, **121**, e2401409121.
40 T. Divoux, E. Agoritsas, S. Aime, C. Barentin, J.-L. Barrat, R. Benzi, L. Berthier, D. Bi, G. Biroli, D. Bonn,

P. Bourrianne, M. Bouzid, E. Del Gado, H. Delanoë-Ayari, K. Farain, S. Fielding, M. Fuchs, J. van der Gucht, S. Henkes, M. Jalaal, Y. M. Joshi, A. Lemaitre, R. L. Leheny, S. Manneville, K. Martens, W. C. K. Poon, M. Popović, I. Procaccia, L. Ramos, J. A. Richards, S. Rogers, S. Rossi, M. Sbragaglia, G. Tarjus, F. Toschi, V. Trappe, J. Vermant, M. Wyart, F. Zamponi and D. Zare, *Soft Matter*, 2024, **20**, 6868–6888.

41 K. Hyun, M. Wilhelm, C. O. Klein, K. S. Cho, J. G. Nam, K. H. Ahn, S. J. Lee, R. H. Ewoldt and G. H. McKinley, *Prog. Polym. Sci.*, 2011, **36**, 1697–1753.

42 C. Storm, J. J. Pastore, F. C. MacKintosh, T. C. Lubensky and P. A. Janmey, *Nature*, 2005, **435**, 191–194.

43 R. C. Ollier, Y. Xiang, A. M. Yacovelli and M. Webber, *Chem. Sci.*, 2023, **14**, 4796–4805.

44 M. L. Gardel, J. H. Shin, F. C. MacKintosh, L. Mahadevan, P. Matsudaira and D. A. Weitz, *Science*, 2004, **304**, 1301–1305.

45 T. Cosgrove, J. Hone, A. M. Howe and R. Heenan, *Langmuir*, 1998, **14**, 5376–5382.

46 C. N. Likos, K. A. Vaynberg, H. Lowen and N. J. Wagner, *Langmuir*, 2000, **16**, 4100–4108.

47 V. Shubin, Y. Samoshina, A. Menshikova and T. Evseeva, *Colloid Polym. Sci.*, 1997, **275**, 655–660.

48 K. Vaynberg, N. J. Wagner, R. Sharma and P. Martic, *J. Colloid Interface Sci.*, 1998, **205**, 131–140.

49 M. Djabourov, K. Nishinari and S. B. Ross-Murphy, *Physical Gels from Biological and Synthetic Polymers*, Cambridge University Press, 2013.

50 H. Kang, Q. Wen, P. Janmey, J. X. Tang, E. Conti and F. C. MacKintosh, *J. Phys. Chem. B*, 2009, **113**, 3799–3805.

51 P. R. Onck, T. Koeman, T. van Dillen and E. van der Giessen, *Phys. Rev. Lett.*, 2005, **95**, 178102.

52 T. B. Goudoulas and N. Germann, *J. Colloid Interface Sci.*, 2019, **556**, 1–11.

53 Y. Séréro, V. Jacobsen and J.-F. Berret, *Macromolecules*, 2000, **33**, 1841–1847.

54 K. Bertula, L. Martikainen, P. Munne, S. Hietala, J. Kleftsrom, O. Ikkala and I. Nonappa, *ACS Macro Lett.*, 2019, **8**, 670–675.

55 A. Sharma, A. J. Licup, R. Rens, M. Sheinman, K. A. Jansen, G. H. Koenderink and F. C. MacKintosh, *Nat. Phys.*, 2019, **12**, 584–587.

56 O. Ronsin, C. Caroli and T. Baumberger, *J. Chem. Phys.*, 2016, **144**, 064904.

57 S. Courty, J. L. Gornall and E. M. Terentjev, *Proc. Natl. Acad. Sci. U. S. A.*, 2005, **102**, 13457–13460.

58 R. D. Groot, A. Bot and W. G. M. Agterof, *J. Chem. Phys.*, 1996, **104**, 9209–9219.

59 E. I. Wisotzki, P. Tempesti, E. Fratini and S. G. Mayr, *Phys. Chem. Chem. Phys.*, 2017, **19**, 12064–12074.

60 E. Nikoumanesh and R. Poling-Skutvik, *J. Chem. Phys.*, 2023, **159**, 044905.

61 E. Nikoumanesh, C. J. M. Jouaneh and R. Poling-Skutvik, *Soft Matter*, 2024, **20**, 7094–7102.

62 S. Mora, *Soft Matter*, 2011, **7**, 4908–4917.

63 M. Bouzid and E. Del Gado, *Langmuir*, 2018, **34**, 773–781.

64 G. J. Donley, M. Bantawa and E. Del Gado, *J. Rheol.*, 2022, **66**, 1287–1304.